

https://doi.org/10.1070/QEL16560

Dynamics and instabilities in long SRS fibre lasers with linear and ring cavities

L.A. Mel'nikov, Yu.A. Mazhirina

Abstract. **We report results of numerical simulation of the nonlinear dynamics of SRS fibre lasers with linear and ring cavity configurations and of the specific features of manifestation of instabilities of steady-state lasing in fibres with length-periodic modulation of dispersion. The simulation is performed within the approach based on solving transport equations. The dynamics of the SRS laser with linear configuration is found to depend strongly on the coupling of counterpropagating waves at the fibre end faces and radically changes in the presence of reflections at the left or right end faces under asymmetric pumping. The existence of signal beatings in the absence of nonreciprocity (rotation) of the cavity and the presence of coupling between counterpropagating waves is demonstrated for the ring laser. A specific feature of instabilities of the propagation regime of a constant-intensity signal in a fibre with a group-velocity dispersion periodically modulated over length is their occurrence at an arbitrary dispersion sign.**

Keywords: *stimulated Raman scattering, counterpropagating waves, transport equations, instabilities, laser gyroscope, group-velocity dispersion, pulse sequence generation.*

1. Introduction

The dynamics of fibre lasers has been studied for a long time. These studies were determined in many respects by new experimental results and possibilities provided by fibres and laser systems of new types. All the time, an important line of research was the analysis of the dynamics of fibre lasers using SRS or SBS pump conversion [1]. In contrast to the lasers based on activated fibres, lasing in SRS or SBS lasers may occur even in the absence of feedback in the cavity (single-pass lasing), because SBS and SRS gains are high even at moderate pump powers, while the loss in fibre is small. The main dynamic effects in SRS or SBS fibre lasers with linear asymmetric configuration (fibre excitation from one end face) are related to the relaxation oscillations arising due to the action of the wave propagating towards the pump wave (SBS lasers) or the Stokes wave copropagating with the pump wave (SRS lasers) [2–4].

These oscillations occur generally with a period equal to the round-trip time of light in the cavity, when the cavity length coincides with the fibre length, or with a period determined by some effective length, when the cavity length is smaller (because of the absorption of pump power) [2]. The fibre dispersion is generally disregarded, since the pulse duration is sufficiently long; however, an important circumstance is that the equations describing lasing are partial differential equations, which cannot be reduced to a system of ordinary equations of low dimension. Therefore, analytical results can be obtained only under rather stringent approximations, which often are not satisfied in experiments [3].

Specifically for this reason numerical experiments play an important role in the analysis of dynamic phenomena [1, 2]. Within the conventional approach, the equations are supplemented with boundary conditions at the fibre end faces (two-point boundary problem, which calls for rather complicated integration methods), and multiple runs over the fibre length are often used to satisfy boundary conditions. All these factors require a long calculation time and analysis of the convergence of successive approximation procedures.

SRS lasers based on long (several tens or hundreds of kilometres) fibres are applied in telecommunication systems as distributed amplifiers [5]. Ring configurations of long fibre lasers are of particular interest, because optical gyroscopic devices can be designed on their basis; note also that, using a long fibre, one can design a cavity with a large scale coefficient, relating the phase delay (caused by rotation) or the difference in the frequencies of counterpropagating waves with the angular rotation speed [6]. In conventional ring lasers, due to the amplitude–phase lasing conditions, the linear coupling of counterpropagating waves with slightly differing frequencies leads to a frequency locking, which impedes the measurement of low rotation speeds, at which the beat frequency becomes comparable with the lock-in zone width.

The lock-in zone width is estimated as Rc/L, where c is the speed of light; c/L is the mode spacing; L is the ring cavity perimeter; and R is the coupling coefficient of counterpropagating waves, which ranges from 10^{-5} to 10^{-6} in gas lasers. In optical fibres, due to the Rayleigh scattering, this coefficient is approximately 10^{-4} (for 1-km-long fibres). However, as was noted above, the SRS generation is not so sensitive to the phase relations for the cavity field; therefore, one can hope to obtain data about rotation even under the conditions of such high backscattering.

Some recent studies, devoted to the dynamics of long fibre lasers, were stimulated by the concept of random feedback in optical fibre [7–10], when generation may occur practically in a single pass in the absence of mirrors upon symmetric fibre excitation [11]. The role of Rayleigh scattering and spontaneous Raman scattering is in the formation of seed fields for SRS, due to which various instabilities may develop.

L.A. Mel'nikov, Yu.A. Mazhirina Yuri Gagarin Saratov State Technical University, ul. Politekhnicheskaya 77, 410054 Saratov, Russia; A.M. Prokhorov General Physics Institute, Russian Academy of Sciences, ul. Vavilova 38, 119991 Moscow, Russia; e-mail: lam-pels@ya.ru

Received 30 October 2017
Kvantovaya Elektronika **47** (12) 1083–1090 (2017)
Translated by Yu.P. Sin'kov

Many problems are related to the analysis of the dynamics of short pulses in long fibre lasers. A number of studies have been published quite recently, where mode locking was obtained in a fibre laser with cavity elements having significantly different dispersions, which leads to the occurrence of the regimes caused by instabilities similar to Faraday (parametric) ones [12]. The propagation regimes of short (picosecond) light pulses in fibres with a dispersion periodically changing over length are also interesting for generating entangled soliton-like pulses [13]. The propagation of waves with constant intensity in optical fibres is known to be accompanied by instability in the case of negative group-velocity dispersion (GVD) [14]; however, similar instabilities are observed for counterpropagating waves and cross-phase modulation even at positive GVD. Modulation of fibre dispersion parameters may also lead to parametric-type instability [15].

To study the processes occurring in these lasers and develop their adequate physical models, it is convenient to consider simplified cavity configurations. Specifically this approach is used in this work. In addition, numerical simulation is performed by solving the transport equations for the field amplitudes of counterpropagating waves applying grid methods and the Courant–Isaacson–Rees algorithm [16], which made it possible to study the laser dynamics for a large number of passes through fibre without applying iterative algorithms.

2. Dynamics of a long SRS laser

2.1. Lasing equations

The equations for the amplitudes of Stokes waves (subscript s) and pump waves propagating along the z (F) axis and in the opposite direction (B), with allowance for the dispersion, have the form [11]

$$\frac{\partial F}{\partial t} + v_g\frac{\partial F}{\partial z} - \frac{\mathrm{i}}{2}D_p\frac{\partial^2 F}{\partial z^2} = -g_R v_g F(|F_s|^2 + |B_s|^2) - \gamma_p v_g F, \quad (1)$$

$$\frac{\partial B}{\partial t} - v_g\frac{\partial B}{\partial z} - \frac{\mathrm{i}}{2}D_p\frac{\partial^2 B}{\partial z^2} = -g_R v_g B(|F_s|^2 + |B_s|^2) - \gamma_p v_g B, \quad (2)$$

$$\frac{\partial F_s}{\partial t} + v_g\frac{\partial F_s}{\partial z} - \frac{\mathrm{i}}{2}D_s\frac{\partial^2 F_s}{\partial z^2} = \bar{g}_R v_g F_s(|F|^2 + |B|^2) - \gamma_s v_g F_s + v_g C^*(z) B_s, \quad (3)$$

$$\frac{\partial B_s}{\partial t} - v_g\frac{\partial B_s}{\partial z} - \frac{\mathrm{i}}{2}D_s\frac{\partial^2 B_s}{\partial z^2} = \bar{g}_R v_g B_s(|F|^2 + |B|^2) - \gamma_s v_g B_s + v_g C(z) F_s, \quad (4)$$

where $\bar{g}_R = g_R\omega_s/\omega_p$ is the Stokes wave gain (in $\mathrm{km^{-1}\ W^{-1}}$); γ_p and γ_s are the loss factors at the pump (ω_p) and Stokes wave (ω_s) frequencies, respectively (in $\mathrm{km^{-1}}$); $v_g = (\mathrm{d}\beta/\mathrm{d}\omega_{p(s)})^{-1}$ is the group velocity; $\beta(\omega_{p(s)})$ is the propagation constant; $D_{p(s)} = (\mathrm{d}^2\beta/\mathrm{d}\omega_{p(s)}^2)^{-1}$ is the dispersion coefficient; and $C(z)$ is the wave coupling coefficient due to the Rayleigh scattering. Since $C(z)$ is proportional to $\exp(2\mathrm{i}\beta_s z_j)$, where z_j is a random coordinate of the jth scatterer [17], for an integration step in z of about 1 m, one can assume this coefficient to have a random phase.

These equations were derived by expanding the waveguide field in spatial harmonics $\exp(\mathrm{i}\beta z)$, in contrast to the conventional approach implying expansion in frequency. This approach makes it possible to solve numerically the Cauchy problem with the initial conditions $F_s(z,0)$, $B_s(z,0)$ and avoid complex computational schemes when setting the input pulse at $z = 0$: $F_s(0,t)$, $B_s(0,t)$. The boundary conditions must be written separately for linear and ring cavities.

The field amplitudes are normalised so as to make the unit amplitude correspond to a power of 1 W.

2.2. Linear cavity

Let us assume that a fibre segment of length L is excited on the left and on the right and that reflection of Stokes waves may occur on its right and left ends. Then we have

$$F_s(0,t) = \sqrt{R_{left}}\,B_s(0,t), \quad B_s(L,t) = \sqrt{R_{right}}\,F_s(L,t), \quad (5)$$

$$F(0,t) = \sqrt{R_{left}}\,B(0,t) + \sqrt{P_{left}}\,,$$
$$B(L,t) = \sqrt{R_{right}}\,F(L,t) + \sqrt{P_{right}}\,. \quad (6)$$

Here, R_{left} and R_{right} are power reflectances on the segment left and right ends, respectively; and P_{left} and P_{right} are pump powers.

2.3. Ring cavity

Let us assume that a fibre segment of length L is rolled into a ring and excited (through a WDM coupler) by waves propagating clockwise (F, F_s) and counterclockwise (B, B_s). We assume also that the coupler is not ideal. As a result, counterpropagating Stokes waves are coupled, and there are no reflections at the pump frequency. Then,

$$F_s(0,t) = \sqrt{R}\,B_s(0,t) + \sqrt{1-R}\,F_s(L,t),$$
$$B_s(L,t) = -\sqrt{R}\,F_s(L,t) + \sqrt{1-R}\,B_s(0,t), \quad (7)$$
$$F(0,t) = F(L,t) + \sqrt{P_{left}}\,, \quad B(L,t) = B(0,t) + \sqrt{P_{right}}\,.$$

2.4. Integration method

It is convenient to perform calculations using normalised coordinates $Z = z/L$ and $T = tv_g/L$. In this case, the equations contain dimensionless linear gains $\bar{g}_R P_{left(right)}L$ and $g_R P_{left(right)}L$ and absorption $\gamma_{p(s)}L$.

Equations (1)–(4) are 'transport' equations:

$$\left(\frac{\partial}{\partial t} \pm \frac{\partial}{\partial z}\right)U(z,t) = V(z,t).$$

It is reasonable to integrate them numerically using the Courant–Isaacson–Rees scheme [16], which can be written as

$$U(z,t) \to U(z_m,t_n) = U_{mn},$$
$$z_m - z_{m-1} = \mathrm{d}z, \quad t_n - t_{n-1} = \mathrm{d}t, \quad \sigma = \mathrm{d}t/\mathrm{d}z, \quad \sigma \leqslant 1,$$
$$U_{m\,n+1} = (1-\sigma)U_{mn} + \sigma U_{m\pm1\,n} + V_{mn}\mathrm{d}t.$$

3. Calculation results

Numerical calculations were performed with the following values of parameters: $g_R = 0.6\ \mathrm{km^{-1}\ W^{-1}}$, $\gamma_p = 0.055\ \mathrm{km^{-1}}$, $\gamma_s = 0.046\ \mathrm{km^{-1}}$, and $L = 22.5$ km. At this fibre length and moderate pump intensities (no higher than the occurrence

threshold for second-order Stokes waves), one can reach values $g_R P_{left}/\gamma_p \approx 100$ and implement regimes in which the pump power is almost completely absorbed in fibre; in addition, this length corresponds to that used in the experiment [11]. At smaller fibre lengths, higher pump intensities are necessary to induce relaxation oscillations [2]. At large lengths, the observed regimes are qualitatively similar to those at a chosen length. Since spontaneous Raman scattering is significant only in the regions characterised by low Stokes-wave intensity (i.e., at the fibre ends), its contribution was modelled by 'illumination' (with a power of 10^{-5} W) of the corresponding fibre end faces (left for t wave F_s and right for the wave B_s).

It was verified that variations in the illumination power at this level do not affect the dynamics of the system. It was also found that scattering on the order of $\sim 10^{-4}$ at a fibre length of 1 km does not affect much the dynamics, and the influence of scattering is similar to that of illumination. Therefore, the $C(z)$ value was assumed to be zero. At the same time, a significant factor for the dynamics is the wave reflections at the fibre end faces. First, if the pump radiation is not completely absorbed throughout the fibre length, a reflected pump wave and the corresponding gain on the counterpropagating wave arise. Second, the power of the Stokes wave reflected from the end face may exceed the illumination power, a circumstance significant for the development of relaxation oscillations.

It was assumed that the pump field is switched on instantaneously at $t = 0$. The pump wave propagates along the z axis, and a copropagating Stokes wave (continuously amplified) travels jointly with it. A counterpropagating Stokes wave is generated in the regions the pump wave arrives at. Both Stokes waves deplete the pump wave. The transient process lasts for ~ 10 passes through the fibre.

Since the characteristic times and spatial scales of field variation in long fibres (on the order of 1 km or more) under pumping with a constant intensity at the fibre input lie in the ranges of several microseconds and several hundreds of meters, respectively, one can neglect dispersion and assume that $D_p, D_s = 0$.

3.1. Linear SRS laser

Let us consider asymmetric pump regimes, where $P_{right} = 0$. Figure 1 shows time dependences of $|F(0.04L, t)|^2$, $|F_s(L, t)|^2$, and $|B_s(0, t)|^2$ for four reflectances on the right end face.

It can be seen that the increase in the reflectance on the right end face leads first to the occurrence of relaxation damping oscillations, which then become regular (an increase in the pump intensity makes them chaotic); however, their period is not equal to that of the cavity round trip. To demonstrate this effect, the pump intensity was modulated at the round-trip frequency. The corresponding beatings can be seen well in Fig. 1d. The intensity oscillation period is about 0.6 of the round-trip time; i.e., a perturbation propagates through a fibre with a velocity exceeding v_g. This occurs when the perturbation penetrates a region with a higher gain amplification, which is characteristic of a Stokes wave counterpropagating with respect to the pump wave.

Figure 2 shows the spatial dependences of intensities at different instants after the transient process for two reflec-

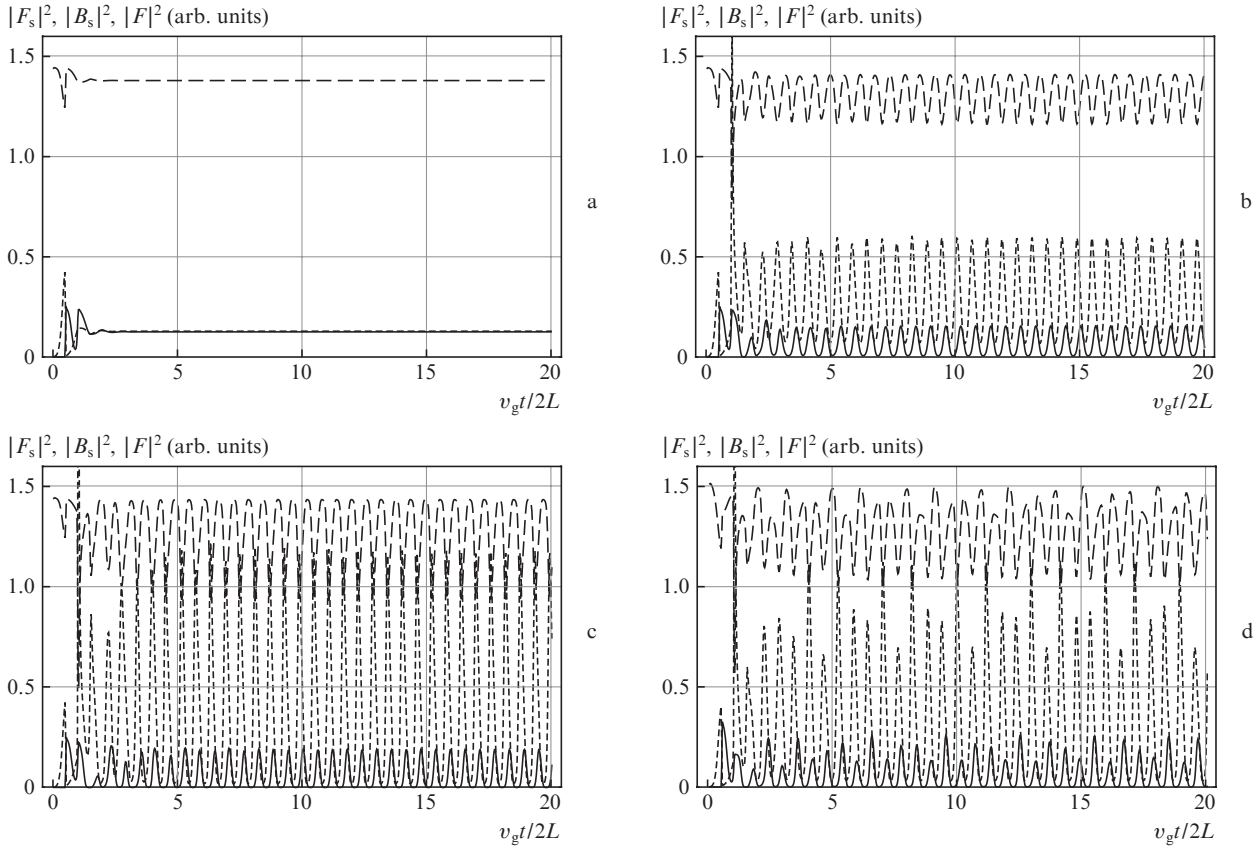

Figure 1. Time dependences of the intensities of forward (solid lines) and backward (short-dash lines) Stokes waves and pump waves (long-dash lines) at R_{right} = (a) 0, (b) 0.0001, (c) 0.005, and (d) 0.0025. The pump modulation depth in Fig. 1d is 0.05; $R_{left} = 0$; $P_{left} = 1.5$ W (a–d).

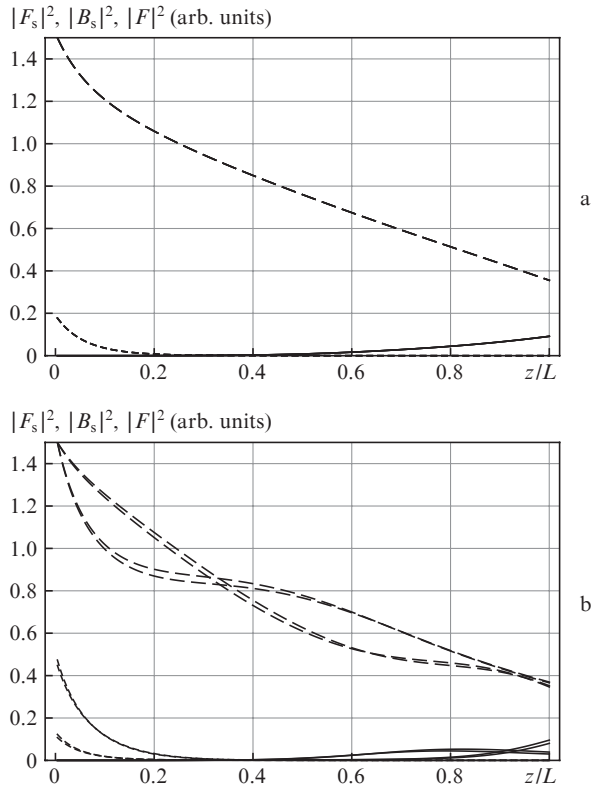

Figure 2. Dependences of Stokes and pump wave intensities on the coordinate at R_{right} = (a) 0.0001 and (b) 0.00075 and R_{left} = (a, b) 0. The curve designations are the same as in Fig. 1.

tances; one of them corresponds to stationary intensities, and the other corresponds to intensity oscillations. In the latter case, the recording interval is 0.3 of the round-trip time, i.e., approximately half oscillation period.

Dependences of the Stokes-wave intensities on the pump level are shown in Fig. 3 for different reflectances of the right fibre end face. The wave intensities were recorded at a specified pump level after the transient process in the interval L/v_g, equal to the wave pass time through the fibre with a step of $L/(20v_g)$. With a change in the pump intensity, the initial conditions for the fields corresponded to the fields in the previous step. One can see well that, beginning with certain pump intensities, the steady-state generation regime becomes unstable, and the intensity of the counterpropagating Stokes wave significantly exceeds that of the wave copropagating with the pump wave.

Figure 4 presents a map of dynamic regimes in the pump level–reflectance plane at the end face, where the boundary between the regimes of steady-state generation and intensity oscillations is shown. The maximum and minimum powers (for the pass time through the fibre) were calculated at a specified pump level and reflectance. When these values coincide, one observes the steady-state regime, while their difference characterises the modulation level. The boundary between the regimes was taken to be the difference between the maximum and minimum powers (in 10^{-4} W). The steady-state regime occurs at pump levels near the threshold; an increase in the pump intensity gives rise to oscillations. Note that the observation threshold for pump intensity oscillations depends weakly on the reflectance. At high intensities, steady-state regimes are observed only at small (on the order of 10^{-4} of less) reflectance values.

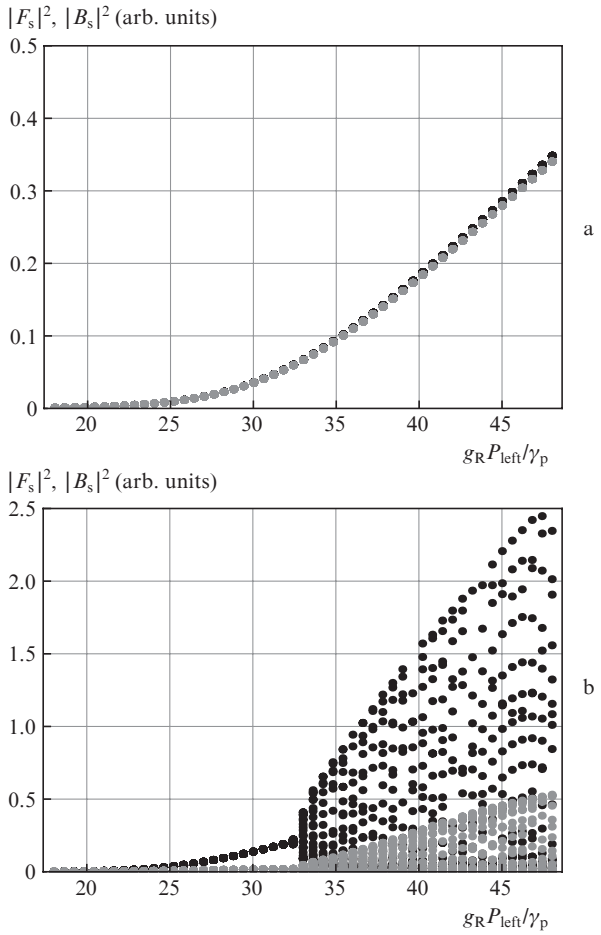

Figure 3. Dependences of the Stokes wave intensities on the pump level at R_{right} = (a) 0 and (b) 0.005 and R_{left} = (a, b) 0. Grey and black circles correspond to forward and backward Stokes waves, respectively.

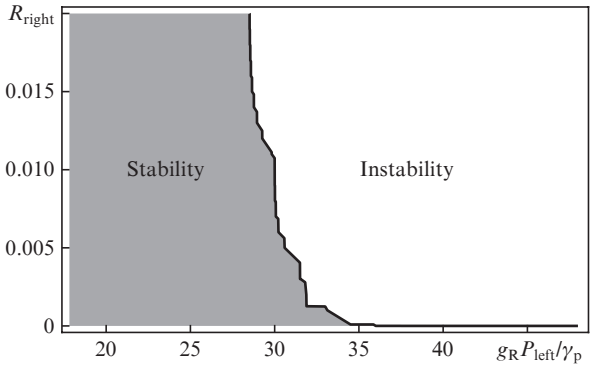

Figure 4. Dynamic-regime map in the case of wave reflection at the right fibre end face.

Since the feedback necessary for the occurrence of oscillations is formed due to the waves B (counterpropagating pump wave) and B_s upon reflection at the right end face, it is interest to consider the reflection at the left end face, when the counterpropagating pump wave does not arise.

It was found that in this case, despite the similarity of dynamic regimes, oscillations occur at much higher pump intensities, and the regions of steady-state and non-steady-state regimes exchange places. This situation is shown in Fig. 5. It was also found that, at identical reflectances at the right

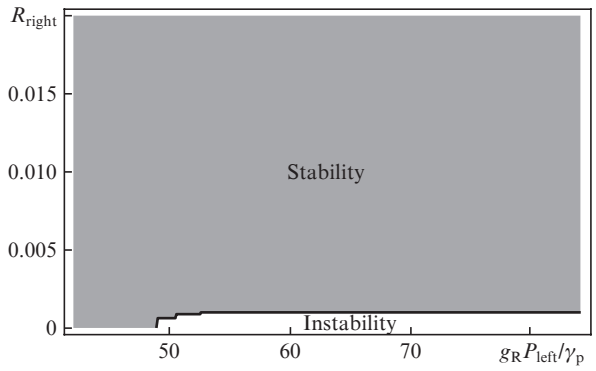

Figure 5. Dynamic-regime map in the case of wave reflection at the left fibre end face.

and left end faces, the regime map virtually completely coincides with that for the reflection at only the left end face; i.e., the reflection at the left end face leads to stabilisation.

To explain this strong asymmetry, we should note the following: in the case of reflection at the right end face, the initial intensity of the counterpropagating Stokes wave B_s is determined by the illumination and reflection of rather strong wave F_s. An increase in the initial intensity leads to a rise in the wave intensity at the left fibre end face and a decrease in the pump wave intensity (generally near the left end face, because the pump intensity at the fibre input is maintained constant). In the absence of reflection at the left end face, the initial wave intensity F_s is determined by only the illumination (spontaneous Raman scattering and Rayleigh scattering). Therefore, the intensity of this wave at the right end face is determined by the amplification under pumping, whose intensity changes both in time and along the fibre length. Any pump wave perturbations propagate jointly with the copropagating Stokes wave; under these conditions, the counterpropagating Stokes wave is generally subjected to the length-integrated pump effect. Thus, a positive feedback is formed to give rise to intensity perturbations. In the absence of reflections at the right end face, the feedback is negative, and oscillations arise only at high pump levels.

These results correspond to the results of numerical simulation and experimental observations in the case of long mirrorless SRS laser [11].

3.2. Ring laser

Let us analyse a ring laser under symmetric pumping, a case where $P_{right} = P_{left}$. We will also take into account the possible nonreciprocity of counterpropagating waves due to the fibre coil rotation. The rotation can be taken into account in the simplest way by supplementing the equation with terms responsible for the nonreciprocal phase delay, $\pm(i/2)\Delta\omega F(F_s)$ and $\pm(i/2)\Delta\omega B(B_s)$. The frequency shift $\Delta\omega$ is proportional to the rotation speed Ω: $\Delta\omega = 8\pi v_g S\Omega/(c\lambda L)$, where S is the fibre coil area and λ is wavelength [6]. The frequencies of the counterpropagating waves are different for the pump waves and Stokes waves.

Figure 6 shows the time dependences of wave intensities. It can be seen that nonreciprocity gives rise to a beat signal, while weak reflection at the coupling element causes periodic power transfer between counterpropagating waves. Generally,

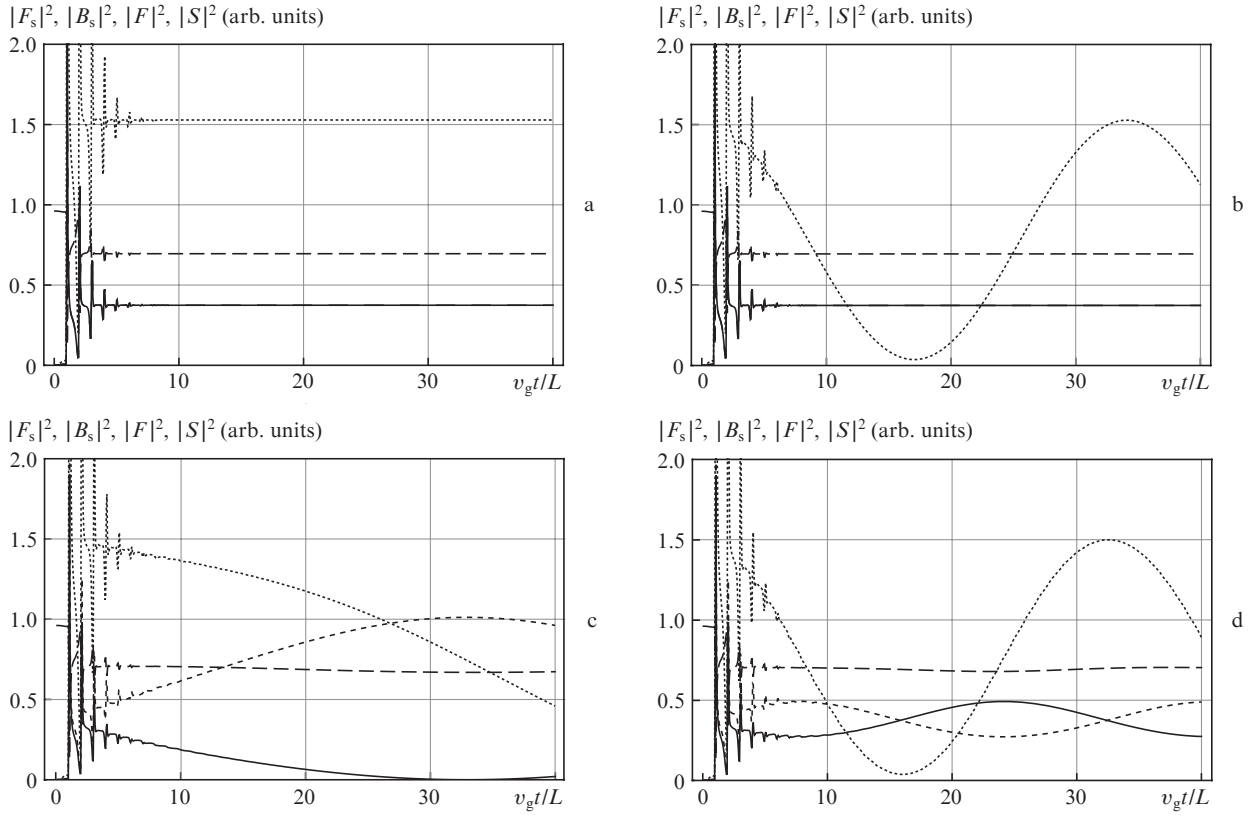

Figure 6. Time dependences of the Stokes and pump wave intensities in a ring laser at R = (a, c) 0 and (b, d) 0.0001 and $\Delta\omega L/(2v_g)$ = (a, c) 0 and (b, d) 0.2. The curve designations are the same as in Fig. 1; the interference signal $|F_s(L,t) + B_s(L,t)|^2 = |S|^2$ is shown by dotted lines.

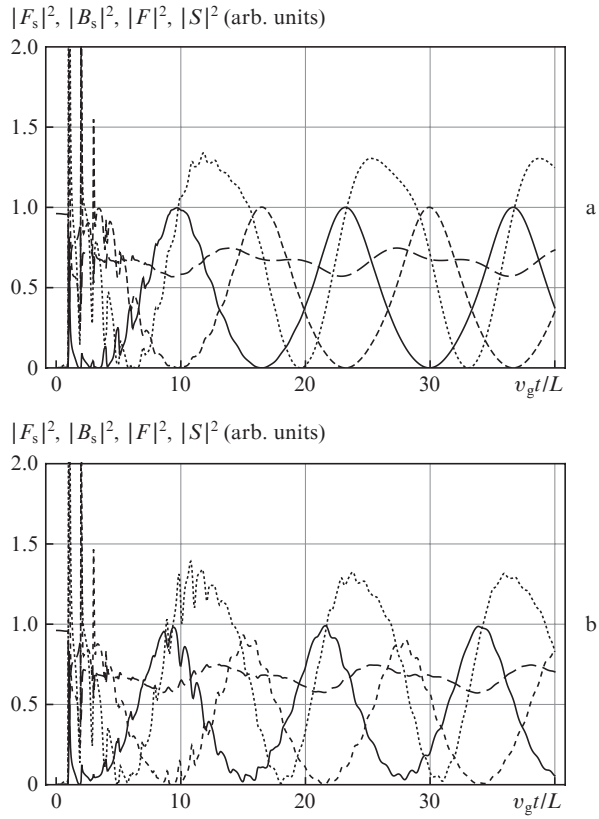

Figure 7. Time dependences of wave intensities and interference signal in a ring laser at $R_{right} = R_{left}$ = (a, b) 0.01 and $\Delta\omega L/v_g$ = (a) 0 and (b) 0.2. The curve designations are the same as in Fig. 6.

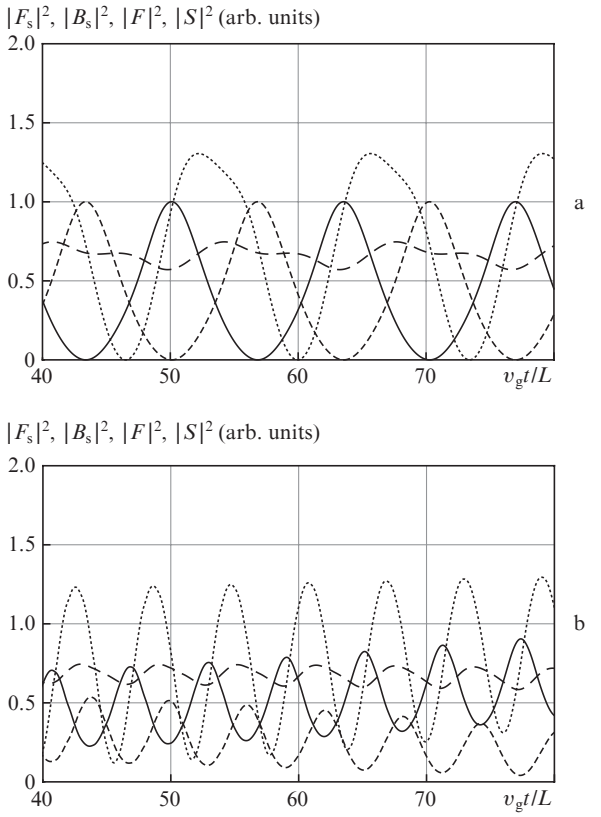

Figure 8. Time dependences of the wave intensities and interference signal after the transient process at $R_{right} = R_{left}$ = (a, b) 0.01 and $\Delta\omega L/v_g$ = (a) 0 and (b) 1.0. The curve designations are the same as in Fig. 6.

an increase in the coupling coefficient leads to an increase in the oscillation frequency (Fig. 7). It can also be seen that relaxation oscillations occur at frequencies close to the cavity round-trip frequency, especially in the beginning of the transient process; however, as in the case of a linear cavity, the frequency of relaxation oscillations by the end of the transient process exceeds the round-trip frequency.

The intensity oscillations due to the linear coupling of counterpropagating waves and the beat signal due to the nonreciprocity (rotation) are interrelated, because not only wave amplitudes but also phases are important under conditions of coherent addition of waves at the coupling element in case of reflection. Figure 8 shows the time dependences of intensities after the transient process. It can be seen that the beat signal exists even in the absence of rotation and that the beat frequency increases when rotation occurs. A change in the rotation sign leads to a rise in the beat frequency. This situation significantly differs from the case of a ring laser, where the beat frequency in the presence of wave coupling is generally lower than in the absence of coupling, and beatings are absent at low rotation speeds (counterpropagating-wave frequencies are locked in). This behaviour is determined by the difference in the conditions for self-excitation and steady-state generation in a conventional laser (where the field returning to the active atom after the cavity round trip should be phase-coupled with the emitted field) and in the case of SRS gain (where the presence of a pump field, whose nonlinear conversion provides Stokes waves, is sufficient). Due to the large SRS-gain linewidth, the phase relations are automatically satisfied for the Stokes modes in a high-Q cavity.

3.3. Dispersion effects

The influence of dispersion manifests itself when the dispersion length $l_d = \tau^2/\beta_2$, where τ is the pulse duration and $\beta_2 = d^2\beta/d\omega^2$ characterises the GVD ([1], Ch. 5), becomes comparable with the fibre length. For the pulses propagating in a fibre laser cavity, an important factor is that the cavity elements periodically affect the pulses multiply passing through the cavity. Recently, Tarasov et al. [13] theoretically and experimentally investigated the operation regimes of an SRS fibre laser in which generation of a sequence of picosecond pulses is observed (with a large number of pulses per cavity length). The cavity of this laser was formed by a fibre with a positive GVD and Bragg fibre gratings having a negative GVD and bias (symmetrically with respect to the frequencies at which spectral reflection bands were generated by centres), so that the cavity GVD was positive as a whole. The occurrence of pulses was interpreted as a parametric (Faraday) instability of the constant-intensity generation regime.

Let us consider the propagation of pulses in a fibre characterised by GVD and Kerr nonlinearity. We assume the GVD to be a periodic function of longitudinal coordinate; this approach models in a sense a laser cavity of the above-considered type. The equation describing the pulse propagation [nonlinear Schrödinger equation (NSE)] can be presented in the conventional form [1]:

$$2i\frac{\partial A(z,t)}{\partial z} - D(z)\frac{\partial^2 A(z,t)}{\partial t^2} + 2\alpha A^2(z,t)A^*(z,t) = 0. \qquad (8)$$

Here, α is the nonlinearity coefficient; $D(z)$ is a parameter responsible for GVD; and the inequality $D > 0$ corresponds to normal dispersion. The propagation of a beam with constant intensity corresponds to the solution to NSE in the form $A(z,t) = \sqrt{P_{\text{left}}}\exp(\mathrm{i}\alpha P_{\text{left}} z)$.

3.4. Instability of steady-state solutions for a fibre with periodic dispersion

Let us consider the stability of this solution. The equations for small deviations

$$A(z,t) = A_0(z,t)\{1 + [x(z)\exp[\mathrm{i}y(z)]]\cos(\Omega t)\}$$

have the form

$$\begin{aligned} 2y'(z) &= \Omega^2 D(z)x(z) + 4P\alpha x(z), \\ 2x'(z) &= -\Omega^2 D(z)y(z), \end{aligned} \tag{9}$$

which is equivalent to the second-order equation

$$x'' = -K^2(z)x + Q(z)x, \tag{10}$$

where

$$K(z) = \sqrt{\frac{1}{4}\Omega^4 D^2(z) + P\alpha\Omega^2 D(z)}; \quad Q(z) = \frac{D'(z)}{D(z)}. \tag{11}$$

For a dispersion constant along the fibre length, $D(z) = D_0$, and $\alpha(z) = \alpha_0$, we obtain the well-known result [1]: at negative GVD ($D_0 < 0$), the wave number of perturbation is imaginary, which corresponds to perturbation amplification (modulation instability). We assume that $D(z) = D_0 + d\cos(2\pi\kappa z)$.

Let us determine the perturbation increment from the formula $g = (2/z_0)\ln[x(z_0)/x(0)]$ for a sufficiently large value $z = z_0$. Having solved numerically the system of equations (10) and (11), one can obtain a frequency dependence for the increment.

The calculation results for $D_0 = \pm 1$ ps^2 km^{-1}, $\alpha = 1$ km^{-1} W^{-1}, $P_{\text{left}} = 1$ W, and $d = 1$ ps^2 km^{-1} are presented in Fig. 9. For comparison, the increment for the case of modulation instability is also shown (grey curve). It can clearly be seen that periodic modulation leads to the occurrence of additional domains of existence of instabilities for both negative and positive GVDs.

Figure 10 shows the calculation results for a more realistic model of dispersion evolution, corresponding to study [13], where a fibre with constant positive dispersion and Bragg fibres with negative GVD were used; i.e., the GVD stepwise changed in the laser. For definiteness, we assume that the negative dispersion region with GVD D_1 covers 10% fibre length:

$$D(z) = \begin{cases} D_0, & 0 \leqslant z \leqslant 0.9L, \\ D_1, & 0.9L < z \leqslant L. \end{cases}$$

It can be seen that instability occurs near a frequency of 10 GHz, which is consistent with the experimental data of [13]. To estimate the characteristic frequency values, it is useful to find the characteristic spatial rate of variation in the parameters of the field modulated at the frequency Ω specified by formula (11) and compare it with the spatial dispersion modulation frequency. At $\Omega/(2\pi) = 10^{-2}$ THz, we obtain a

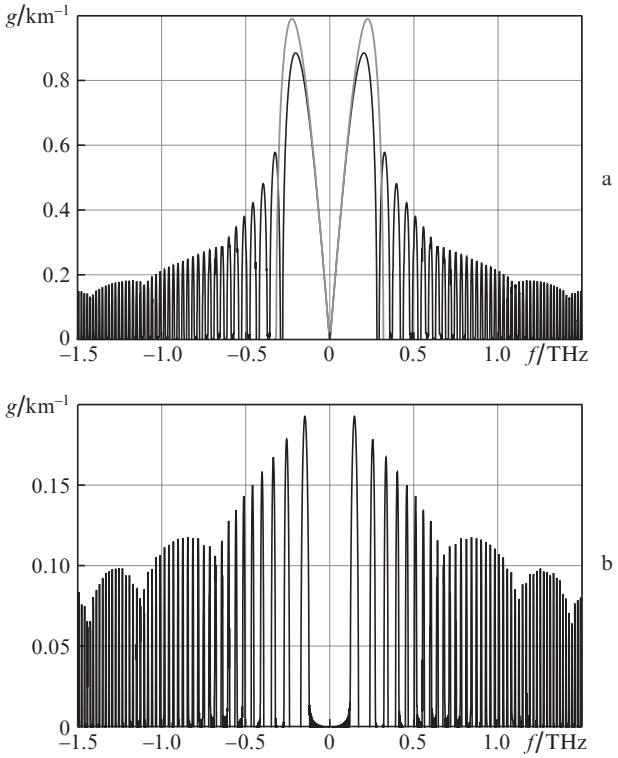

Figure 9. Dependences of the perturbation increment g on frequency f for (a) negative and (b) positive GVDs at $D_0 = \pm 1$ ps^2 km^{-1}, $\alpha P_{\text{left}} = 1$ km^{-1}, and $d = 1$ ps^2 km^{-1}. The grey and black curves correspond to constant ($d = 0$) and alternating dispersions, respectively.

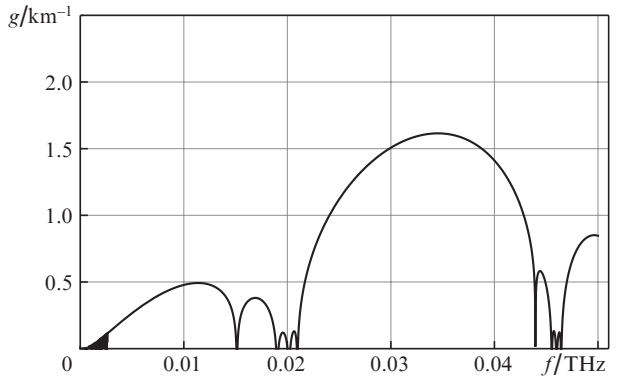

Figure 10. Dependence of the instability increment g on frequency f for a step dispersion at $L = 2.2$ km, $D_0 = 25$ ps^2 km^{-1}, $D_1 = -240$ ps^2 km^{-1}, and $\alpha P_{\text{left}} = 6$ km^{-1}.

spatial modulation period of about 3 km, which is also consistent with the experimental data of [13].

Figure 11 shows the spatiotemporal dynamics of instability development, which was obtained by solving numerically Eqn (8) with conventional normalisation of the longitudinal coordinate to the dispersion length and the time to the pulse width. The dispersion was assumed to be varied along the fibre length. Under this normalisation, one can assume that $D_0 = 1$ or -1. The modulation amplitude was sufficiently large ($d = 2$), a situation corresponding to the formation of regions with different GVD signs over fibre length; the spatial modulation frequency was $\kappa = 0.2\pi$. The frequency of perturbations (time modulation against the constant intensity background) was taken to be equal to κ ($v_g = 1$). It can be seen that an

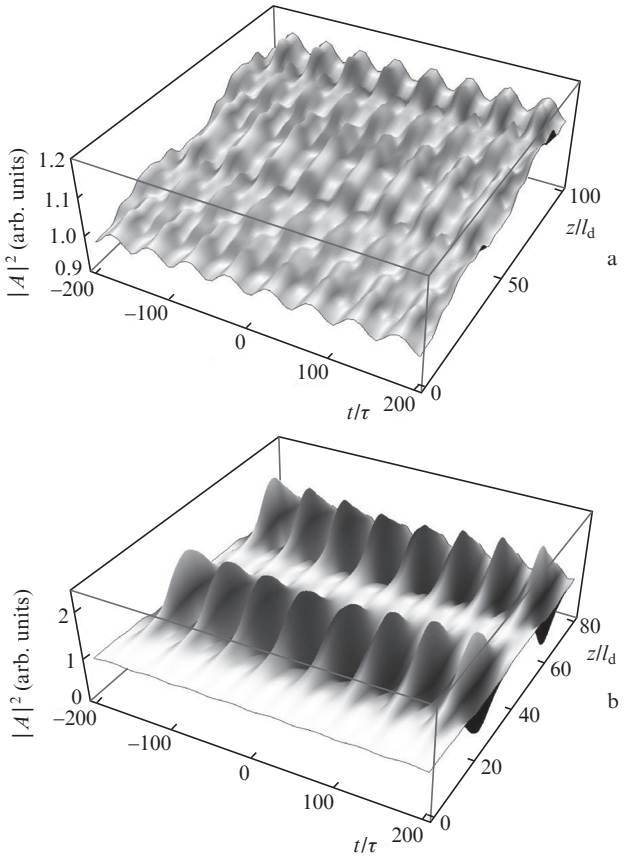

Figure 11. Spatiotemporal dynamics of instability development for $D_0 =$ (a) 1 and (b) –1, $d = 2$, and $\kappa = 0.2\pi$.

instability at positive GVD leads to the generation of pulses that periodically change places when propagating against the background of a large constant signal. In the case of negative GVD, soliton-like pulses are generated.

4. Conclusions

We performed a numerical simulation of the nonlinear dynamics of SRS fibre lasers with linear and ring cavity configurations and the specific features of manifestation of instabilities of the steady-state generation regime in fibres with dispersion periodically modulated over their length. The use of transport theory approaches in the simulation allowed us to propose and implement an efficient numerical algorithm, making it possible to trace the laser system dynamics for long times, corresponding to several tens or hundreds of passes through the cavity.

It was shown for a linear laser that the dynamics of an asymmetrically pumped system depends strongly on which of the fibre end faces the counterpropagating Stokes waves are coupled.

The ring laser demonstrated the presence of a beat signal in the absence of rotation and a change in the beat frequency with a change in the angular rotation speed.

The instabilities of the constant-intensity signal propagation regime in a fibre with GVD periodically modulated over length, which exist at an arbitrary dispersion sign, were analysed.

Acknowledgements. The part of the work concerning the dynamics of ring SRS lasers was supported in part by the Ministry of Education and Science of the Russian Federation (Project No. 9.2108.2017/PCh), and the part dealing with the instabilities in fibres with periodic group-velocity dispersion was supported by the Russian Science Foundation (Project No. 17-12-01564).

References

1. Agraval G.P. *Nonlinear Fiber Optics* (Waltham: Academic Press, 2013).
2. Jhonson R.V., Marburger J.H. *Phys. Rev. A*, **4**, 1175 (1971).
3. Bar-Joseph I. *J. Opt. Soc. Am. B*, **2**, 1606 (1985).
4. Narum P. *J. Opt. Soc. Am. B*, **5**, 623 (1988).
5. Ania-Castañón et al. *Phys. Rev. Lett*., **101**, 123903 (2008).
6. Melnikov L.A. et al. *Proc. Symposium Gyro Technology* (Karlsruhe, Germany, 2011) Vol. 8, p. 7.
7. Churkin D.V. et al. *Nat. Commun*., **6**, 6214 (2015).
8. Churkin D.V. *Nat. Commun*., **6**, 7004 (2015).
9. Turitsyna E.G. et al. *Nat. Photonics*, **7**, 783 (2013).
10. Aragoneses A. et al. *Phys. Rev. Lett*., **116**, 033902 (2016).
11. Mazhirina Yu.A. et al. *Prikl. Nelineinaya Din*., **22**, 73 (2014).
12. Perego A.M. et al. *Phys. Rev. Lett*., **116**, 028701 (2016).
13. Tarasov N. et al. *Nat. Commun*., **7**, 12441 (2016).
14. Konukhov A.I. *Laser Phys*., **12**, 055103 (2015).
15. Conforti M. et al. *Phys. Rev. Lett*., **116**, 028701 (2016).
16. Love J.D., Snyder A.W. *Optical Waveguide Theory* (New York: Chapman and Hall, 1983; Moscow: Radio i Svyaz', 1987).
17. Courant R., Isaacson E., Rees M. *Commun. Pure Appl. Math*., **5**, 243 (1952).